Intermolecular interaction in the OH^+–He and OH^+–Ne open-shell ionic complexes: Infrared predissociation spectra of the ν_1 and $\nu_1 + \nu_b$ vibrations

Doris Roth, Sergey A. Nizkorodov, John P. Maier, and Otto Dopfer[a)]
Institut für Physikalische Chemie, Universität Basel, Klingelbergstrasse 80, CH-4056 Basel, Switzerland

Midinfrared spectra of the OH^+–He/Ne open-shell ionic complexes have been recorded by photofragmentation spectroscopy in a tandem mass spectrometer. The ν_1 vibration (OH stretch) and its combination band with the intermolecular bending vibration ($\nu_1 + \nu_b$) have been observed for both complexes at the level of rotational resolution. The analysis of the spectra shows that both complexes have a linear proton-bound structure in their $^3\Sigma^-$ electronic ground states, with intermolecular center-of-mass separations of 2.60 and 2.65 Å for OH^+–He and OH^+–Ne, respectively. The ν_1 vibrational origins are redshifted by 66.3 and 169.9 cm^{-1} with respect to the corresponding monomer transition indicating that the intermolecular interaction increases upon ν_1 excitation. The fine structure of the ν_1 ($^3\Sigma^- \leftarrow {}^3\Sigma^-$) and $\nu_1 + \nu_b$ ($^3\Pi \leftarrow {}^3\Sigma^-$) transitions arising from electron spin and vibrational angular momentum of ν_b have been analyzed in terms of a semirigid Hamiltonian including spin–spin, spin–rotation, and l-type doubling interaction terms. The molecular parameters extracted from the molecular constants provide valuable information on the radial and angular part of the intermolecular potential-energy surface in each considered vibrational state. The intermolecular interaction in OH^+–Ne is stronger than in OH^+–He, mainly due to the larger polarizability of the rare-gas atom. © *1998 American Institute of Physics.* [S0021-9606(98)00434-6]

I. INTRODUCTION

The accurate knowledge of inter- and intramolecular potential-energy surfaces is essential for the understanding of many important physical, chemical, and biological processes and properties of molecules and clusters. The main experimental sources of information about potential-energy surfaces of complexes are high-resolution spectroscopic studies.[1–6] In contrast to weakly bound neutral clusters containing closed-shell molecules, such experimental data are rare for neutral open-shell complexes.[6–12] In the case of open-shell ionic molecular complexes they are practically nonexistent, with the notable exception of a recent microwave study on H_2^+–He.[13] However, open-shell species are interesting from the chemical point of view as they often feature high reactivities and appear as transient intermediates in reactions.[14] The present work reports the first observation of rotationally resolved infrared (IR) spectra of the open-shell OH^+–He and OH^+–Ne complexes. The analysis contributes to a better understanding of intermolecular interactions in weakly bound open-shell ionic species.

The OH^+ ion, serving as the IR chromophore in the OH^+–Rg clusters, is of interest in many environments such as oxygen and hydrogen containing plasmas, earth upper atmosphere, and interstellar space.[15–18] The $^3\Sigma^-$ electronic ground state of OH^+ has been well characterized by microwave,[19,20] far-infrared,[21–23] midinfrared,[18,24] and UV spectroscopy,[25] and by *ab initio* calculations.[26–32] Experiments on various isotopic species[19–21,23,25] revealed an interatomic separation of $r_e = 1.0279$ Å and a harmonic fre-

quency of $\omega_e = 3113.37$ cm^{-1}.[23,25] In addition to the electronic ground state, several excited states have been studied both experimentally[25,33,34] and theoretically.[29–32]

To date there have been no spectroscopic studies on complexes involving the open-shell OH^+ ion and neutral ligands. The only source of spectral information for such species is a recent *ab initio* calculation on several electronic states of OH^+–He.[35] It predicts a linear proton-bound geometry for the $^3\Sigma^-$ ground state with a He–H separation of 1.572 Å, a binding energy $D_0 = 3.8$ kJ/mol (≈ 300 cm^{-1}) and harmonic frequencies $\omega_1 = 3017$ cm^{-1}, $\omega_s = 242$ cm^{-1}, and $\omega_b = 291$ cm^{-1} for the intramolecular OH stretch and the intermolecular stretch and bend vibrations, respectively.

The purpose of the present work is to furnish spectroscopic data on the simple triatomic OH^+–He and OH^+–Ne complexes by means of infrared predissociation spectroscopy. These efforts continue a series of systematic investigations on similar AH^+–Rg complexes where A is a closed-shell diatomic molecule (N_2, CO) and Rg a rare-gas atom (He, Ne, Ar).[36–42] Rotationally resolved infrared spectra revealed that these clusters possess linear proton-bound equilibrium structures, in agreement with recent microwave data[43] and *ab initio* calculations.[35,44–48] However, the OH^+–Rg complexes differ in two ways from the previously studied AH^+–Rg systems. First, as OH^+ is an open-shell ion, the spectra of OH^+–Rg complexes are complicated by the effects of electron spin interaction, which provide useful information on the angular part of the intermolecular potential.[10] Second, they are triatomic systems and therefore the number of vibrational degrees of freedom is reduced to only four. Thus OH^+–Rg clusters are attractive model systems from the theoretical point of view, as the calculation of

---

[a)]Author to whom correspondence should be addressed; electronic mail: dopfer@ubaclu.unibas.ch

full-dimensional potential-energy surfaces at high levels of theory is feasible. Especially OH^+–He with its small number of electrons may serve as a prototype system (similar to H_2^+–He)[13] to study intermolecular interactions in weakly bound, open-shell ionic complexes. The spectra presented in the present work initiated *ab initio* and rovibrational calculations for OH^+–He and OH^+–Ne, where two-dimensional intermolecular potential-energy surfaces were created for the $\nu_1 = 0$ and $\nu_1 = 1$ vibrational states taking the intramolecular OH coordinate into account in an adiabatic way.[48]

II. EXPERIMENT

Midinfrared photofragmentation spectra of mass selected OH^+–Rg complexes with Rg=He/Ne were recorded in a tandem mass spectrometer. The experimental setup and the spectroscopic technique have been described previously.[38,49,50]

The parent complexes OH^+–He (OH^+–Ne) were produced in an electron impact ion source by coexpanding a mixture of O_2, H_2, and He (and Ne) in a ratio of approximately 1:1:100 (1:1:100:100) at a stagnation pressure of 5–8 bar through a pulsed nozzle. The chemistry of O_2 and H_2 containing rare-gas discharges has been discussed previously.[24,51] It was found that low concentrations of O_2 and H_2 favor the production of OH^+ and H_2O^+ compared to the more stable closed-shell H_3O^+ ion. Mass spectra of the ion distribution in the employed electron impact supersonic expansion source reflected this behavior indicating that the chemistry in this source is quite similar to that in a discharge cell.

The first quadrupole mass spectrometer (QMS) selected the parent complexes from the variety of (cluster) ions present in the skimmed supersonic beam. After 90° deflection, the mass-selected OH^+–Rg beam was injected into an octopole ion guide where it was overlapped in space and time with a counterpropagating infrared laser pulse. Transitions into metastable rovibrational levels of the complex induced its fragmentation into the Rg atom and OH^+ ion, as the internal excitation after absorption exceeded the lowest dissociation threshold of the complex. A second QMS transmitted only OH^+ fragment ions which were subsequently measured by an ion detector. Thus photofragmentation spectra of OH^+–He/Ne complexes were obtained by monitoring the OH^+ fragment current as a function of the excitation frequency.

Infrared radiation was generated by a Nd–YAG laser pumped optical parametric oscillator (OPO) system featuring a 0.02 cm^{-1} bandwidth, 2500–6800 cm^{-1} tuning range, 5 ns pulse width, 20 Hz repetition rate, and 0.5–5 mJ/pulse energy (depending on the frequency range). Calibration was accomplished by recording etalon markers of the OPO oscillator (free spectral range 4 GHz) and optoacoustic absorptions of HDO with the signal output of the OPO. Line positions in the photofragmentation spectra were corrected for the Doppler shift induced by the kinetic energy of the ions in the octopole (≈ 2 to 3 eV). The absolute accuracy of the calibration is limited to 0.01 cm^{-1} by a combination of the

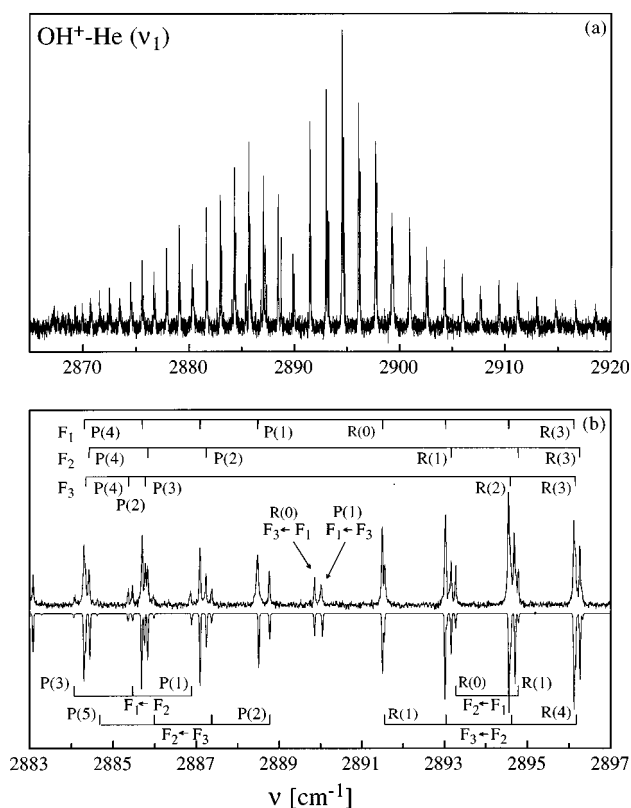FIG. 1. (a) Infrared photodissociation spectrum of the ν_1 vibration of OH^+–He. (b) Comparison of experimental (top) and simulated (bottom, 24 K) ν_1 spectrum near the band origin with assignments.

uncertainty in the ion's kinetic energy (± 0.5 eV) and the laser resolution.

III. RESULTS

A. OH^+–He

The midinfrared predissociation spectrum of OH^+–He was investigated in the vicinity of the OH^+ fundamental ($\nu_1 \approx 2956$ cm^{-1}) to locate the corresponding transition of the complex and possible combination bands involving intermolecular vibrations. Two transitions were found in the frequency range 2590–3710 cm^{-1}. The first band with origin at 2890 cm^{-1} is redshifted by 66 cm^{-1} with respect to the monomer ν_1 frequency, and has the rotational structure expected for a $^3\Sigma \leftarrow {}^3\Sigma$ transition of a linear molecule (Fig. 1). It is therefore attributed to the ν_1 fundamental of the complex. The second band centered at 3093 cm^{-1} appears 203 cm^{-1} to the blue of the ν_1 transition of the complex and has a structure characteristic for a linear molecule $^3\Pi \leftarrow {}^3\Sigma$ transition (Fig. 2). Consequently, it is assigned to the $\nu_1 + \nu_b$ combination band.

The following Hamiltonian has been employed for the analysis of the rotational and electron spin fine structure of the $^3\Sigma$ states (i.e., the ground and ν_1 vibrational states):[52]

$$\hat{H} = B\hat{N}^2 - D\hat{N}^4 + \tfrac{2}{3}\lambda(3\hat{S}_z^2 - \hat{S}^2) + \gamma\hat{N}\hat{S}. \tag{1}$$

The first two terms correspond to the rotational and centrifugal distortion energies, whereas the other two terms account for the spin–spin and spin–rotation interaction arising from
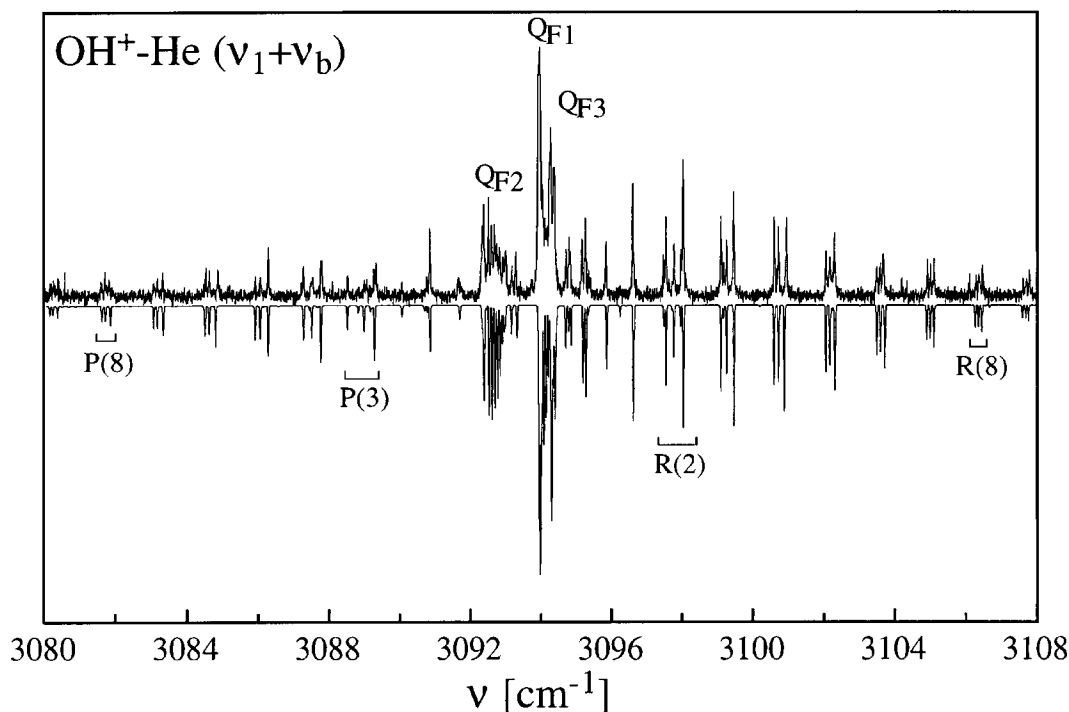
FIG. 2. Infrared photodissociation spectrum of the $\nu_1 + \nu_b$ vibration of OH$^+$–He (top) compared to a simulation assuming $T = 30$ K (bottom).

the electron spin. The rotational dependencies of λ and γ (λ_D and γ_D) as well as the sextic centrifugal distortion constant (H) were found unnecessary for the present experimental accuracy. Following Hund's case (b), in a $^3\Sigma$ vibronic state the electron spin momentum $\hat{S}$ couples with the rotational angular momentum $\hat{N}$ ($\hat{N} = \hat{R}$ for a Σ state) to form the total angular momentum $\hat{J} = \hat{N} + \hat{S}$.[53] Thus in a triplet state ($S = 1$) each J level (with $J \geq 1$) is split into three sublevels F_1, F_2, and F_3 with total angular momentum $J = N+1$, $J = N$, and $J = N-1$, respectively.

In the case of the $^3\Pi$ vibronic state (i.e., $\nu_1 + \nu_b$), additional terms appear in the Hamiltonian due to the vibrational angular momentum $\hat{l}$ of the intermolecular bending motion which couples with the rotational momentum $\hat{R}$ to $\hat{N} = \hat{R} + \hat{l}$:[52]

$$\hat{H} = B\hat{N}^2 - D\hat{N}^4 + \tfrac{2}{3}\lambda(3\hat{S}_z^2 - \hat{S}^2) + \gamma\hat{N}\hat{S} + \gamma_G\hat{N}_z\hat{S}_z$$
$$- \tfrac{1}{2}o_G(\hat{S}_+^2 + \hat{S}_-^2) - \tfrac{1}{2}q_G(\hat{N}_+^2 + \hat{N}_-^2)$$
$$+ \tfrac{1}{2}p_G(\hat{N}_+\hat{S}_+ - \hat{N}_-\hat{S}_-). \tag{2}$$

For $l = 1$, l-type doubling (described by the parameters o_G, p_G, and q_G) splits each level of a Σ state ($l = 0$) further into two sublevels (e and f), i.e., in a $^3\Pi$ state each J level (with $J \geq 2$) is split into six sublevels. Similar to the case of the $^3\Sigma$ states, the λ_D, γ_D, and H constants as well as the l-type doubling parameter p_G could not be determined for the $^3\Pi$ states. The Hamiltonians used for both the $^3\Sigma$ and $^3\Pi$ vibronic states have been diagonalized using the program PGOPHER.[54]

The selection rules for allowed rovibrational transitions in a $^3\Sigma \leftarrow ^3\Sigma$ band are $\Delta J = \pm 1$ and $\Delta N = \Delta J$ giving rise to P and R branch lines, each of which is split into three com-

ponents ($F_i \leftrightarrow F_i$, $i = 1-3$). Indeed, the ν_1 transition of OH$^+$–He shows such a structure (Fig. 1). In total, 88 transitions were observed between 2870 and 2920 cm^{-1} and assigned to the ν_1 band of OH$^+$–He, with P and R branch lines ranging from $P(17)$ to $R(16)$ employing the notation $\Delta N(N)$. Except for the $P(2)$ and $P(3)$ lines, for which the triplet fine structure is completely resolved, all P and R branch lines appeared as doublets due to the overlap of the F_1 and F_3 components. In addition, several forbidden transitions with $\Delta N = \pm 1$, $\Delta N \neq \Delta J$, and $F_i \leftrightarrow F_j$ ($i \neq j$) were observed for low N ($N \leq 5$) with decreasing intensity for increasing N: $F_3 \leftarrow F_1$ $R(0)$; $F_2 \leftarrow F_1$ $R(0,1)$; $F_3 \leftarrow F_2$ $R(1,4,5)$; $F_1 \leftarrow F_3$ $P(1)$; $F_1 \leftarrow F_2$ $P(1-4)$; and $F_2 \leftarrow F_3$ $P(2-4)$. The detection of these transitions strongly facilitated the assignments and considerably improved the accuracy of the determined fine-structure constants.

The selection rules for allowed rovibrational transitions in a $^3\Pi \leftarrow ^3\Sigma$ vibronic band are $\Delta J = 0, \pm 1$ and $\Delta N = \Delta J$ which give rise to P, Q, and R branch lines, each of which is again split into three components ($F_i \leftrightarrow F_i$, $i = 1-3$) by the electron spin interaction. Q branch lines follow the $f \leftrightarrow e$ selection rule, whereas P and R branch transitions combine only e or f levels (i.e., $e \leftrightarrow e$ and $f \leftrightarrow f$). The $\nu_1 + \nu_b$ band of OH$^+$–He centered at 3094 cm^{-1} features in fact three strong Q branches confirming the $^3\Pi \leftarrow ^3\Sigma$ character of this transition. In contrast to the ν_1 band, the triplet fine structure in the P and R branches of the $\nu_1 + \nu_b$ transition is completely resolved. In total, 77 isolated lines have been assigned ranging from $R(0)-R(9)$, $P(2)-P(9)$, and $Q(1)-Q(10)$. The following forbidden lines have been identified: $F_2 \leftarrow F_1$ $R(0-2)$ and $Q(1)$; $F_3 \leftarrow F_2$ $R(1)$ and $Q(2)$; $F_1 \leftarrow F_2$ $Q(2,5)$; $F_2 \leftarrow F_3$ $P(3)$ and $Q(1)$.

The molecular constants of the vibrational ground state

TABLE I. Molecular constants (in cm^{-1}) of OH$^+$–He and OH$^+$–Ne in several vibrational levels of the $^3\Sigma^-$ electronic ground state obtained from line positions in the respective photofragmentation spectra. The corresponding values of OH$^+$ are listed for comparison.

		OH$^+$ [a]	OH$^+$–He [b]	OH$^+$–Ne [b]
Ground	B	16.422 86(7)	0.73427(9)	0.25648(5)
state	D	$1.9218(8)\times10^{-3}$	$4.69(3)\times10^{-5}$	$2.24(5)\times10^{-6}$
	λ	2.1434(6)	1.584(3)	1.780(8)
	γ	$-0.151\,08(17)$	-6.75×10^{-3} [c]	-2.36×10^{-3} [c]
ν_1		2956.3561(10) [d]	2890.061(4)	2786.500(2)
	$\Delta\nu_1$		66.295(4)	169.856(2)
	B	15.695 26(6)	0.74674(6)	0.260 44(2)
	D	$1.8732(8)\times10^{-3}$	$3.96(2)\times10^{-5}$	$1.71(2)\times10^{-6}$
	λ	2.1331(5)	1.712(3)	1.847(1)
	γ	$-0.146\,57(15)$	-6.97×10^{-3} [c]	-2.43×10^{-3} [c]
$\nu_1+\nu_b$			3093.456(7)	3114
	ν_b		203.395(8)	327
	B		0.7385(4)	
	D		$7.8(4)\times10^{-5}$	
	λ		0.840(9)	
	γ		-6.75×10^{-3} [e]	
	γ_G		$-0.13(1)$	
	o_G		0.847(9)	
	q_G		0.0066(2)	

[a]Reference 24.
[b]Line positions are available upon request. The accuracy of absolute line positions is about 0.01 cm^{-1}.
[c]Fixed at the values calculated from relation (3).
[d]Shifted by $+4/3\times(\lambda'-\lambda'')$ compared to Ref. 24 to be compatible with the ν_1 origin definition used in the present work.
[e]Fixed at the value of the ground state.

of OH$^+$–He listed in Table I were obtained from a least-squares fit of 84 combination differences, derived from both the ν_1 and $\nu_1+\nu_b$ transitions, to those calculated from the Hamiltonian of Eq. (1). As the accuracy of the experimental data was not sufficient to determine the spin–rotation constant γ, it was fixed at the value obtained by scaling the monomer value with the ratios of the respective rotational constants according to

$$\gamma_{\text{OH}^+\text{–Rg}}=\gamma_{\text{OH}^+}\times\frac{B_{\text{OH}^+\text{–Rg}}}{B_{\text{OH}^+}}. \qquad (3)$$

The standard deviation of the fit, 0.013 cm^{-1}, is of the order of the experimental resolution (0.02 cm^{-1}), and all observed combination differences (including those determined from overlapping transitions) could be reproduced by the constants of Table I to better than 0.035 cm^{-1}. Floating the spin–rotation constants γ in the fit did not change the other constants within the standard deviation. Moreover, ground-state molecular constants derived from a global fit of all observed transition frequencies were less accurate than those extracted from combination differences because of perturbations in the ν_1 state (see below).

The constants of the ν_1 state were determined by fitting the observed ν_1 transition frequencies, whereby the lower state constants were fixed at the values derived from combination difference analysis. Preliminary fits revealed that the upper-state levels with $N'=6$ are slightly perturbed leading to a systematic deviation of up to 0.040 cm^{-1} between observed and calculated $R(5)$ and $P(7)$ transition fre-

quencies. This local perturbation was also evident from reduced intensities of the transitions accessing the perturbed energy levels in both P and R branches. These lines, as well as transitions with overlapping F_1 and F_3 components, were therefore excluded from the fit. Fitting 56 isolated transitions to Hamiltonian (1) resulted in the molecular constants of the ν_1 excited state listed in Table I, with a standard deviation of 0.010 cm^{-1}. All observed transition frequencies including overlapping and perturbed lines could be reproduced by these constants to within 0.045 cm^{-1}. Figure 1(b) compares the experimental ν_1 spectrum near the band origin with a simulation utilizing the constants of Table I and a Boltzmann distribution with a temperature of $T=24$ K. This temperature was derived from a Boltzmann plot for low N levels. Higher N levels had a population corresponding to a much higher temperature of roughly 130 K. In agreement with previous observations,[55] the efficiency of rotational cooling in the employed ion source decreases for levels with increasing rotational energy leading to nonthermal rotational distributions.

The $\nu_1+\nu_b$ state molecular constants listed in Table I were derived from a least-squares fit of all observed transitions to those calculated from Hamiltonians (1) and (2) for the lower and upper state, respectively, whereby the ground-state constants were again fixed at the values obtained from the combination differences. The upper-state spin–rotation constant γ was fixed at the ground-state value. As Q branch transitions terminate at different sublevels of the l doublet than the P and R branch lines, the observation of isolated resolved Q branch lines allowed the determination of the
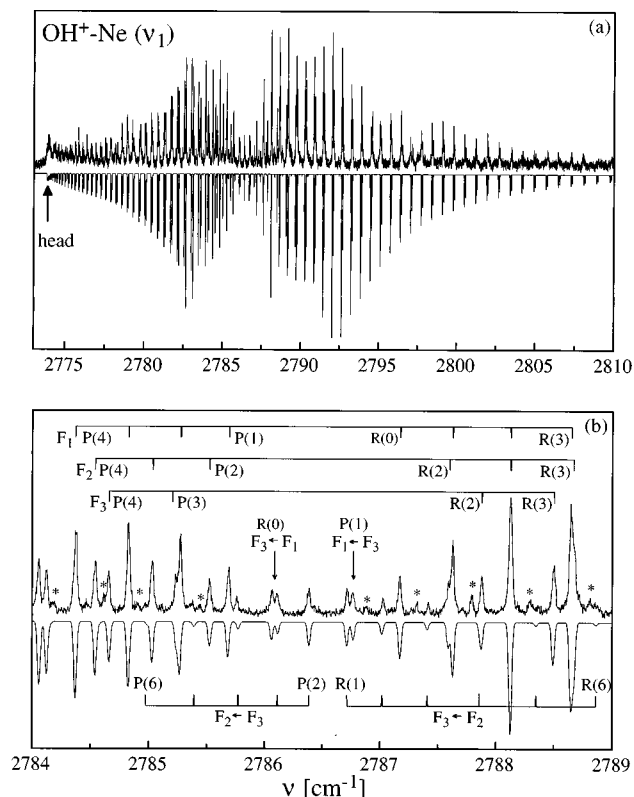
FIG. 3. (a) Infrared photodissociation spectrum of the ν_1 vibration of OH$^+$–Ne (top) and a simulation (bottom) assuming a triple Boltzmann distribution (see text). (b) Comparison of experimental (top) and simulated (bottom, 42 K) ν_1 spectrum near the band origin with assignments. The asterisks mark lines of the less abundant OH$^+$–^{22}Ne isotopomer.

l-type doubling parameters o_G and q_G. Figure 2 shows the spectrum simulated with constants derived from the fit (standard deviation$=0.024$ cm^{-1}) and a single temperature of 30 K.

B. OH$^+$–Ne

The midinfrared predissociation spectrum of the OH$^+$–Ne complex (only the ^{20}Ne containing isotopomer was investigated in detail) was measured in the spectral range 2660–4140 cm^{-1}, and similar to OH$^+$–He two transitions
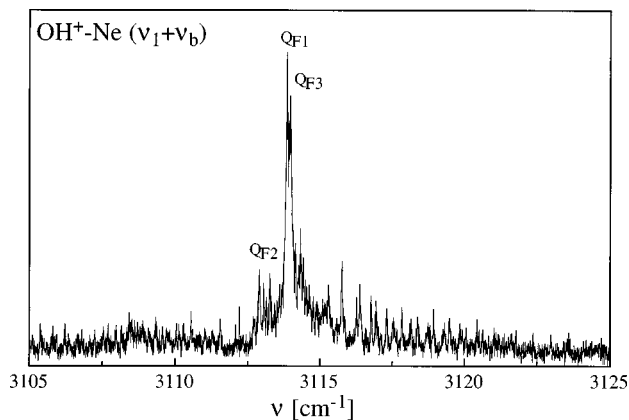

FIG. 4. Infrared photodissociation spectrum of the $\nu_1+\nu_b$ vibration of OH$^+$–Ne.

have been detected. A $^3\Sigma\leftarrow{}^3\Sigma$ type band with origin at 2786.5 cm^{-1}, i.e., 170 cm^{-1} to the red of the free OH$^+$ stretch frequency, is assigned to the ν_1 fundamental of the OH$^+$–Ne complex (Fig. 3). By analogy to OH$^+$–He, the observed $^3\Pi\leftarrow{}^3\Sigma$ type band appearing 327 cm^{-1} above ν_1 (at 3114 cm^{-1}) is attributed to the $\nu_1+\nu_b$ combination band of OH$^+$–Ne (Fig. 4). Both bands have been analyzed in a similar manner as the corresponding OH$^+$–He transitions.

In total, 155 transitions have been observed in the spectral range 2775–2805 cm^{-1}, and 134 of them have been assigned to $P(28)$ to $R(26)$ lines of the ν_1 band of the OH$^+$–^{20}Ne complex. The remaining lines, marked with asterisks in Fig. 3(b), belong to the ν_1 transition of the less abundant OH$^+$–^{22}Ne isotopomer. Their relative intensities compared to the OH$^+$–^{20}Ne lines are compatible with the natural abundance of ^{22}Ne ($\approx9\%$). Moreover, the rotational analysis as well as the small ν_1 frequency redshift upon $^{20/22}$Ne substitution (0.3 cm^{-1}) confirm their assignment to OH$^+$–^{22}Ne. Transitions of both isotopomers appear in the photodissociation spectrum recorded in the OH$^+$ fragment channel, as the mass resolution of the first QMS was somewhat reduced in order to improve the transmission and consequently the signals of OH$^+$–^{20}Ne. In the remaining part of the paper, only the OH$^+$–^{20}Ne isotopomer will be considered. The contraction of the intermolecular bond upon ν_1 excitation results in the formation of a P branch head at approximately 2773.8 cm^{-1} [$\approx P(42)$]. The triplet fine structure of the band is resolved for several lines near the origin, namely $R(4–6)$, $P(3–5)$, and $P(10–14)$, whereas the other lines in the P and R branch appear as doublets due to two overlapping fine-structure components [Fig. 3(b)]. The detection of several forbidden lines near the band origin [$F_3\leftarrow F_1$ $R(0)$, $F_3\leftarrow F_2$ $R(1–10)$, $F_1\leftarrow F_3$ $P(1)$, $F_2\leftarrow F_3$ $P(2–6)$] is again valuable for the determination of the spin–spin constants.

For the determination of the molecular constants of the ground and ν_1 vibrational levels the spin–rotation constants γ were again held fixed at the values calculated from relation (3). The ground-state constants listed in Table I were obtained by fitting 79 lower-state combination differences (solely derived from the ν_1 band) to Hamiltonian (1) with a standard deviation of 0.011 cm^{-1}, and they could reproduce all ground-state combination differences to better than 0.03 cm^{-1}.

Preliminary fits of the transition frequencies revealed that the upper-state levels with $N'=13–18$ are perturbed resulting in systematic deviations of up to 0.07 cm^{-1} between experimental and calculated $R(12–17)$ and $P(14–19)$ line positions. Exclusion of these perturbed transitions left 136 transition frequencies for the least-squares fit to Hamiltonian (1) giving rise to the ν_1 state molecular constants listed in Table I. The standard deviation of the fit was 0.009 cm^{-1}, and all unperturbed lines could be reproduced with deviations below 0.03 cm^{-1}. Figure 3(a) shows a simulated ν_1 spectrum using the constants from Table I and a triexponential Boltzmann distribution with temperatures $T_1=30$ K (weight 10), $T_2=70$ K (weight 1), and $T_3=150$ K (weight 2). Such a nonequilibrium distribution was necessary to reproduce the intensity profile over the whole band. Figure

TABLE II. Molecular parameters (in cm^{-1}, Å, N/m) of OH$^+$–He and OH$^+$–Ne in several vibrational levels are compared to calculated values (Ref. 48). The experimental values are derived from the molecular constants in Table I via various approximations which are outlined in the text.

State	Parameter[a]	OH$^+$–He		OH$^+$–Ne	
		Expt.[b]	Calc.	Expt.[b]	Calc.
Ground state	R_{CM}	2.6018(2)	2.647	2.6536(3)	2.688
	r_{H-Rg}	1.6230(2)			1.6748(3)
	ω_s / ν_s	179.6(6)/-	-/153	172(2)/-	-/151
	k_s	6.16(4)		16.1(4)	
	$\langle \cos^2 \theta \rangle$	0.826(1)	0.9068	0.887(3)	0.9381
	$\langle \theta \rangle$	24.7(2)°		19.6(3)°	
	ω_b / ν_b	198/-	-/152	295/-	-/249
ν_1	$\Delta \nu_1$	66.295(4)[c]	56	169.856(2)[c]	164
	R_{CM}	2.5761(1)	2.619	2.6320(1)	2.644
	r_{H-Rg}	1.5748(1)		1.6307(1)	
	ω_s / ν_s	200.1(5)/-	-/168	202(1)/-	-/171
	k_s	7.65(4)		22.0(3)	
	$\langle \cos^2 \theta \rangle$	0.868(1)	0.9286	0.9106(4)	0.9544
	$\langle \theta \rangle$	21.3(2)°		17.4(1)°	
	ω_b / ν_b	250/203.395(8)[c]	-/190	381/327[c]	-/319
$\nu_1 + \nu_b$	R_{CM}	2.5911(7)	2.652		
	r_{H-Rg}	1.5898(7)			
	$\langle \cos^2 \theta \rangle$	0.596(3)	0.6463		
	$\langle \theta \rangle$	39.5(3)			

[a]$R_{CM} = \langle 1/R^2 \rangle^{-1/2}$, $\langle \theta \rangle = \arccos(\langle \cos^2 \theta \rangle^{1/2})$.
[b]Quoted errors correspond to standard deviations of the parameters derived from the fits and/or subsequently used equations. They do not reflect the accuracy of the employed approximations.
[c]Measured values.

3(b) shows the spectrum near the band origin including assignments and a comparison with the simulated spectrum ($T = 42$ K).

Figure 4 shows the $\nu_1 + \nu_b$ spectrum of the OH$^+$–Ne complex. Though in several parts of the spectrum single rotational lines were clearly discernible, the limited signal-to-noise ratio and the spectral congestion prevented unambiguous assignments of the observed transitions, and thus a detailed rotational and fine-structure analysis. However, some conclusions can be drawn from the course structure of the spectrum. Similar to the corresponding spectrum OH$^+$–He (Fig. 2) three strong Q branches are apparent confirming the assignment of the band to a $^3\Pi$-$^3\Sigma$ type transi-

TABLE III. Correlation between redshifts of ν_1 frequencies (in cm^{-1}) of AH$^+$–Rg (Rg=He/Ne) complexes, their intermolecular binding energies (in cm^{-1}), and the proton affinities of A (kj/mol).

AH$^+$	PA (A)[a]	AH$^+$–He		AH$^+$–Ne	
		$\Delta \nu_1$	D_0	$\Delta \nu_1$	D_0
N$_2$H$^+$	495	76[b]	434[d]	181[g]	795[g]
HCO$^+$	594	12[c]	242[e]	43[h]	438[h]
OH$^+$	486	66	360[f]	170	810[f]

[a]References 61 and 62.
[b]Reference 39.
[c]Reference 36.
[d]Reference 47.
[e]D_e value (Ref. 46).
[f]Reference 48.
[g]Reference 40.
[h]Reference 37.

tion. The origin of the transition lies at 3114 cm^{-1} resulting in an intermolecular bending frequency of 327 cm^{-1} in the intramolecular ν_1 state.

IV. DISCUSSION

The molecular constants extracted from the infrared spectra of OH$^+$–He and OH$^+$–Ne can be used to derive geometrical, energetic, and dynamical parameters of the intermolecular potential in the three considered vibrational states. They are summarized in Table II where they are compared with theoretical results obtained in Ref. 48.

Though the rotational structures of the observed vibrational transitions reveal that complexes of OH$^+$ with the rare-gas atoms He and Ne complexes possess (quasi-)linear geometries, the rotational constants do not directly indicate whether the rare-gas atom binds preferentially to the proton or the oxygen end of OH$^+$. However, the significant redshifts in the OH stretch vibration upon complexation point towards a proton-bound linear equilibrium configuration, in agreement with the *ab initio* calculations.[35,48] In addition, linear proton-bound minimum geometries have been found previously for related complexes that are composed of protonated linear closed-shell molecules (HCO$^+$ or HN$_2^+$) and rare-gas atoms. It has been suggested that the redshift of the ν_1 (A–H stretch) frequency in AH$^+$–Rg complexes is related to the difference in the proton affinities (PA) of the two bases A and Rg.[37] For example, for Rg–HCO$^+$ complexes a linear dependence of the ν_1 shift upon the PA of the Rg atom has been observed. As atomic oxygen and molecular nitrogen have similar proton affinities, complexes of OH$^+$ and

N_2H^+ with He and Ne feature comparable binding energies and ν_1 frequency shifts (Table III). In contrast, the higher proton affinity of CO (compared to O and N_2) causes the intermolecular bonds in $Rg–HCO^+$ complexes to be weaker and the ν_1 redshifts to be smaller. The experimental ν_1 redshifts of $OH^+–Rg$ complexes are in close agreement with the theoretical values (Table II).

The assignment of the observed $^3\Pi \leftarrow {}^3\Sigma$ transitions 203 and 327 cm^{-1} to higher frequency of the respective ν_1 transitions of $OH^+–He$ and $OH^+–Ne$ as $\nu_1 + \nu_b$ combination bands is not only justified from symmetry and band profile considerations, but also from the good agreement with the theoretically predicted intermolecular bending frequencies of 190 and 319 cm^{-1} in the respective ν_1 states (Table II). The combination bands with the intermolecular stretching vibration, $\nu_1 + \nu_s$, are also expected to lie in the investigated spectral range. However, besides the ν_1 transition no further $^3\Sigma \leftarrow {}^3\Sigma$ band could be found, indicating that their intensity must be at least a factor 10 lower compared to the $\nu_1 + \nu_b$ transitions. In fact, unrestricted MP2 calculations carried out for $OH^+–He$ (GAUSSIAN 94,[56] aug-cc-pVTZ basis set[57]) predict the transition moment of ν_s to be more than one order of magnitude lower than that of ν_b, consistent with the experimental observation. According to the predicted binding energies (D_0) of 416 and 974 cm^{-1} for $OH^+–He$ and $OH^+–Ne$,[48] the scanned frequency ranges cover for both complexes the whole bound part of the intermolecular potential in the ν_1 excited state. Therefore the $\nu_1 + \nu_b$ combination band is apparently the only strong IR transition from the vibrational ground state involving ν_1 and intermolecular vibrational excitations.

In addition to the vibrational complexation shifts, the molecular constants derived from the analysis of the rotational and electron spin fine structure provide insight into some characteristics of the intermolecular potential-energy surface in the considered vibrational states. Geometrical parameters, such as the average intermolecular center-of-mass separations $R_{CM} = \langle 1/R^2 \rangle^{-1/2}$, and harmonic values for the intermolecular stretching frequency (ω_s) and force constant (k_s) can be derived following a pseudodiatomic harmonic approach assuming that the monomer geometry is not affected upon formation of the complex (Table II).[58] *Ab initio* calculations confirm that indeed the OH^+ bond length (r_e) is only slightly prolonged in the complexes with He (by ≈ 0.005 Å) and Ne (by ≈ 0.01 Å).[48] Intermolecular separations $R_{H–Rg}$ derived from R_{CM} of the complex and OH bond lengths of $r_{v=0} = 1.0405$ Å and $r_{v=1} = 1.0644$ Å are also presented in Table II. The shorter intermolecular bond lengths and larger intermolecular stretching force constants and frequencies in the ν_1 states compared to the respective ground vibrational states indicate that for both complexes the intermolecular interaction increases upon ν_1 excitation. As the interaction of OH^+ with Ne is stronger than that with He, the intermolecular stretching force constants are larger as well. However, in spite of the stronger bonds in the Ne containing complexes, the intermolecular separations $R_{H–Rg}$ are comparable due to the larger van der Waals radius of Ne.

After the discussion of the radial part of the intermolecular interaction, the angular anisotropy of the intermolecular

potential-energy surface is considered. The zero-point angular excursion in each vibrational state can roughly be estimated from the complexation-induced changes in the spin–spin interaction constants[9]

$$\frac{\lambda_{OH^+–Rg}}{\lambda_{OH^+}} = \langle P_2(\cos\theta) \rangle = \frac{1}{2}(3\langle \cos^2\theta \rangle - 1). \qquad (4)$$

The derived angles $\langle\theta\rangle = \arccos(\langle\cos^2\theta\rangle^{1/2})$ of 25° and 20° for the ground states of $OH^+–He$ and $OH^+–Ne$ (Table II) show that the lighter He atom undergoes larger zero-point bending angular excursions in a more isotropic potential. The slightly smaller angles in the respective ν_1 states (21°,17°) indicate that vibrational excitation increases for both complexes not only the radial bond strength but also the angular rigidity. As expected, the average angle increases even further when the bending mode is excited ($\langle\theta\rangle = 40°$ for the $\nu_1 + \nu_b$ state of $OH^+–He$). The smaller harmonic force constant of the intermolecular bending mode in the ν_1 state of $OH^+–He$ ($k_b = 2.5 \times 10^{-20}$ Nm) compared to $OH^+–Ne$ ($k_b = 6.7 \times 10^{-20}$ Nm) also reflects the larger angular anisotropy of the interaction in the latter complex.

In the harmonic approximation, the frequency of the bending vibration (ω_b) is related to the angular elongation by

$$\langle\theta^2\rangle = \frac{h}{4\pi^2 cI\omega_b}, \qquad (5)$$

where I corresponds to the reduced moment of inertia of the complex.[39] Bending frequencies calculated from the angles derived from the spin–spin constants and the approximation $\cos^2\theta \approx 1 - \theta^2$ are listed in Table II, together with measured values and those obtained from rovibrational calculations. The harmonic values for both $OH^+–He$ and $OH^+–Ne$ are significantly (30% and 20%) above the experimental frequencies due to the significant anharmonicities and angular-radial couplings. As the interaction is stronger and more anisotropic in $OH^+–Ne$, the agreement between harmonic and fundamental frequencies is better for the Ne containing complex.

In general, the potential parameters extracted from the experimental molecular constants agree well with those predicted from the rovibrational calculations (Table II), although the comparison may suggest for both complexes a slight systematic underestimation of the interaction strength in the theoretical calculations. Considering only the most directly comparable properties, one observes that the experimental ν_1 redshifts are somewhat larger and the intermolecular center-of-mass separations are somewhat smaller than the respective theoretical values. The comparison between estimated intermolecular stretching frequencies (ω_s and ν_s) also points in the same direction. However, as the experimental values have been estimated in the harmonic approximation while the theoretical ones were obtained by averaging over the respective (ro)vibrational wave functions, part of the discrepancy may arise from the neglect of anharmonicities and angular-radial couplings, as well as other approximations in the evaluation of the experimental parameters.

The linewidths measured for isolated rovibrational lines in both the ν_1 and $\nu_1 + \nu_b$ states of both studied complexes

(≤ 0.03 cm^{-1}) are close to the laser bandwidth of 0.02 cm^{-1}. Thus only a lower limit of the lifetime of the excited metastable rovibrational states of ≈ 200 ps can be derived. Interestingly, for the related N_2H^+–He complex which has a bond strength similar to OH$^+$–He, lifetimes of 38, 76, and 19 ps have been measured for the ν_1, $\nu_1 + \nu_b$, and $\nu_1 + \nu_s$ vibrational levels, indicating that the relaxation processes are relatively fast and also highly mode-selective (i.e., not statistical).[39] Thus it appears that in the case of OH$^+$–He the coupling between intra- and intermolecular degrees of freedom is much weaker for comparable binding and excitation energies. This is most probably due to the lower density of available background states (dark bath states) in OH$^+$–He compared to N_2H^+–He, as there are less intramolecular vibrational degrees of freedom and the intermolecular frequencies are higher due to the smaller reduced mass. Moreover, in the case of the OH$^+$–He complex, the released energy has to be partitioned in either fragment kinetic energy or OH$^+$ rotational excitation. Both processes are inefficient, as they involve large changes in the effective quantum numbers of the respective degrees of freedom (energy gap law).[59,60] In contrast, predissociation of the metastable ν_1 or $\nu_1 + \nu_b / \nu_s$ levels of N_2H^+–He can result in vibrationally excited N_2H^+ fragments (e.g., ν_2), thus significantly decreasing the kinetic-energy release and N_2H^+ rotational excitation and therefore shortening the predissociation lifetime.

Finally, possible origins for the perturbations affecting some of the rovibrational levels of the ν_1 states of the OH$^+$–He/Ne complexes are considered. As was mentioned in Sec. IV the transitions into the $\nu_1 = 1$, $N' = 6$ state of OH$^+$–He and the $\nu_1 = 1$, $N' = 13$–18 states of OH$^+$–Ne have reduced intensities and systematically shifted frequencies. This observation suggests that these levels interact with other quasibound states of the respective complexes. The occurrence of such perturbations in intramolecular vibrational states of weakly bound atom-diatom systems such as OH$^+$–He (Ne) is unusual and somewhat surprising. The lowest bound electronically excited state of OH$^+$ lies more than 2 eV above the electronic ground state[30] and complexation with He (or Ne) is not expected to significantly change this large energy gap. Thus the dark state interacting with the ν_1 fundamental of OH$^+$–He at ≈ 2900 cm^{-1} must be purely intermolecular in nature, with more than 2500 cm^{-1} of energy in excess of the lowest dissociation threshold of the complex ($D_0 = 360$ cm^{-1} for OH$^+$–He).[48] Moreover, the fact that levels close to the $N' = 6$ level of the ν_1 state OH$^+$–He are not affected by the perturbation implies a relatively sharp resonance. Possible candidates for such long-lived dark states are levels that involve a high degree of excitation in the intermolecular bending coordinate. As the barrier for internal rotation is around 300 cm^{-1},[48] levels with excitation energy of the order of 3000 cm^{-1} have practically free internal rotor character. Such states may couple only weakly to the dissociation continuum and possess therefore the required long lifetimes. In addition, the interaction between ν_1 and the free rotor states is not expected to be efficient, in agreement with the experimental observations.

V. CONCLUSIONS

The infrared predissociation spectra of the ν_1 and $\nu_1 + \nu_b$ vibrations of OH$^+$–He/Ne recorded in the present work represent the first high-resolution spectra of weakly bound open-shell ionic complexes in $^3\Sigma$ electronic states. The vibrational frequencies, the complexation-induced frequency shifts, and the molecular rotational and fine-structure constants provide detailed information about the intermolecular interaction potential in the three considered vibrational states. Both complexes possess a linear proton-bound equilibrium geometry with the intermolecular bond being stronger and more rigid in OH$^+$–Ne compared to OH$^+$–He. As the proton affinity of O is close to the one of N_2, the complexes of OH$^+$ and N_2H^+ with He and Ne feature similar intermolecular interaction properties, manifested in comparable binding energies, ν_1 frequency shifts, radial intermolecular stretching force constants, and intermolecular separations. The correlation between proton affinities and ν_1 redshifts in AH$^+$–Rg systems allows a rough estimation of the ν_1 frequency in OH$^+$–Ar as 1900 ± 200 cm^{-1}. This value is below the scanning range of the employed OPO laser, and may also lie below the dissociation energy of the complex. The ν_1 band of OH$^+$–Ar seems therefore to be an ideal candidate for the observation in direct absorption by approaches similar to that applied recently to N_2H^+–Ar.[42] The molecular constants obtained from the present IR spectra of OH$^+$–He/Ne may serve as a useful guideline for searches in the microwave spectral range in order to improve the accuracy of the molecular parameters. Such a strategy was successful in the case of HCO$^+$-Ar.[38,43] Accurate spectroscopic data of OH$^+$–He might also be useful in testing high-level full-dimensional *ab initio* potential calculations that have become feasible for atom-diatom systems. Improvements in both experimental and theoretical directions should lead to a better understanding of the interaction in open-shell ionic systems.

ACKNOWLEDGMENTS

[1] K. R. Leopold, G. T. Fraser, S. E. Novick, and W. Klemperer, Chem. Rev. **94**, 1807 (1994).
[2] D. J. Nesbitt, Annu. Rev. Phys. Chem. **45**, 367 (1994).
[3] R. C. Cohen and R. J. Saykally, J. Phys. Chem. **96**, 1024 (1992).
[4] J. M. Hutson, Annu. Rev. Phys. Chem. **41**, 123 (1990).
[5] Z. Bacic and R. E. Miller, J. Phys. Chem. **100**, 12945 (1996).
[6] R. W. Randall, C.-C. Chuang, and M. I. Lester, Chem. Phys. Lett. **200**, 113 (1992).
[7] M. C. Heaven, Annu. Rev. Phys. Chem. **42**, 283 (1992).
[8] M. C. Heaven, J. Phys. Chem. **97**, 8567 (1993).
[9] H.-B. Qian, D. Seccombe, and B. J. Howard, J. Chem. Phys. **107**, 7658 (1997).
[10] H.-B. Qian, S. J. Low, D. Seccombe, and B. J. Howard, J. Chem. Phys. **107**, 7651 (1997).
[11] H. Meyer, J. Chem. Phys. **107**, 7732 (1997).
[12] C. C. Carter and T. A. Miller, J. Chem. Phys. **107**, 3447 (1997).
[13] A. Carrington, D. I. Gammie, A. M. Shaw, S. M. Taylor, and J. M. Hutson, Chem. Phys. Lett. **260**, 395 (1996).
[14] R. A. Loomis and M. I. Lester, Annu. Rev. Phys. Chem. **48**, 643 (1997).

[15] D. Smith, Chem. Rev. **92**, 1473 (1992).

[16] C. Fehrenbach and C. Arpigny, C. R. Acad. Sci. Paris, Ser. B **277**, 569 (1973).

[17] W. T. Huntress, Astrophys. J., Suppl. **33**, 495 (1977).

[18] M. W. Crofton, R. S. Altman, M.-F. Jagod, and T. Oka, J. Phys. Chem. **89**, 3614 (1985).

[19] Y. K. Bae, Chem. Phys. Lett. **180**, 179 (1991).

[20] P. Verhoeve, J. P. Bekooy, W. L. Meerts, J. J. Ter Meuwlen, and A. Dynamus, Chem. Phys. Lett. **125**, 286 (1986).

[21] M. H. W. Gruebele, R. P. Müller, and R. J. Saykally, J. Chem. Phys. **84**, 2489 (1986).

[22] D.-J. Liu, W.-C. Ho, and T. Oka, J. Chem. Phys. **87**, 2442 (1987).

[23] M. Gruebele, E. Keim, A. Stein, and R. J. Saykally, J. Mol. Spectrosc. **131**, 343 (1988).

[24] B. D. Rehfuss, M.-F. Jagod, L.-W. Xu, and T. Oka, J. Mol. Spectrosc. **151**, 59 (1992).

[25] A. J. Merer, D. N. Malm, R. W. Martin, M. Horani, and J. Rostas, Can. J. Phys. **53**, 251 (1975).

[26] H.-J. Werner, P. Rosmus, and E.-A. Reinsch, J. Chem. Phys. **79**, 905 (1983).

[27] P. Rosmus and W. Meyer, J. Chem. Phys. **66**, 13 (1977).

[28] L. Adamowicz, J. Chem. Phys. **89**, 6305 (1988).

[29] D. M. Hirst and M. F. Guest, Mol. Phys. **49**, 1461 (1983).

[30] D. R. Yarkony, J. Phys. Chem. **97**, 111 (1992).

[31] R. De Vivie, C. M. Marian, and S. D. Peyerimhoff, Chem. Phys. **112**, 349 (1987).

[32] R. P. Saxon and B. Liu, J. Chem. Phys. **85**, 2099 (1986).

[33] D. J. Rodgers and P. J. Sarre, Chem. Phys. Lett. **143**, 235 (1988).

[34] T. D. Varberg, K. M. Evenson, and J. M. Brown, J. Chem. Phys. **100**, 2487 (1994).

[35] J. M. Hughes and E. I. von Nagy-Felsobuki, J. Phys. Chem. A **101**, 3995 (1997).

[36] S. A. Nizkorodov, J. P. Maier, and E. J. Bieske, J. Chem. Phys. **103**, 1297 (1995).

[37] S. A. Nizkorodov, O. Dopfer, M. Meuwly, J. P. Maier, and E. J. Bieske, J. Chem. Phys. **105**, 1770 (1996).

[38] S. A. Nizkorodov, O. Dopfer, T. Ruchti, M. Meuwly, J. P. Maier, and E. J. Bieske, J. Phys. Chem. **99**, 17118 (1995).

[39] M. Meuwly, S. A. Nizkorodov, J. P. Maier, and E. J. Bieske, J. Chem. Phys. **104**, 3876 (1996).

[40] S. A. Nizkorodov, M. Meuwly, J. P. Maier, O. Dopfer, and E. J. Bieske, J. Chem. Phys. **108**, 8964 (1998).

[41] S. A. Nizkorodov, Y. Spinelli, E. J. Bieske, J. P. Maier, and O. Dopfer, Chem. Phys. Lett. **265**, 303 (1997).

[42] T. Speck, H. Linnartz, and J. P. Maier, J. Chem. Phys. **107**, 8706 (1997).

[43] Y. Ohshima, Y. Sumiyoshi, and Y. Endo, J. Chem. Phys. **106**, 2977 (1997).

[44] A. Nowek and J. Leszczynski, J. Chem. Phys. **105**, 6388 (1996).

[45] M. Kolbuszewski, Chem. Phys. Lett. **244**, 39 (1995).

[46] O. Dopfer (unpublished).

[47] M. Meuwly and R. J. Bemish, J. Chem. Phys. **106**, 8672 (1997).

[48] M. Meuwly, J. P. Maier, and P. Rosmus, J. Chem. Phys. **109**, 3850 (1998), following paper.

[49] E. J. Bieske, J. Chem. Soc., Faraday Trans. **91**, 1 (1995).

[50] E. J. Bieske, S. A. Nizkorodov, F. R. Bennett, and J. P. Maier, J. Chem. Phys. **102**, 5152 (1995).

[51] M. W. Crofton, R. S. Altman, M. F. Jagod, and T. Oka, J. Phys. Chem. **89**, 3614 (1985).

[52] S. A. Beaton and J. M. Brown, J. Mol. Spectrosc. **183**, 347 (1997).

[53] H. Lefebvre-Brion and R. W. Field, *Perturbations in the Spectra of Diatomic Molecules* (Academic, New York, 1986).

[54] M. E. Green and C. M. Western, J. Chem. Phys. **104**, 848 (1996).

[55] R. V. Olkhov, S. A. Nizkorodov, and O. Dopfer, J. Chem. Phys. **107**, 8229 (1997).

[56] M. J. Frisch, G. W. Trucks, H. B. Schlegel, P. M. W. Gill, B. G. Johnson, M. A. Robb, J. R. Cheeseman, T. Keith, G. A. Petersson, J. A. Montgomery, K. Raghavachari, M. A. Al-Laham, V. G. Zakrzewski, J. V. Ortiz, J. B. Foresman, J. Cioslowski, B. B. Stefanov, A. Nanayakkara, M. Challacombe, C. Y. Peng, P. Y. Ayala, W. Chen, M. W. Wong, J. L. Andres, E. S. Replogle, R. Gomperts, R. L. Martin, D. J. Fox, J. S. Binkley, D. J. Defrees, J. Baker, J. P. Stewart, M. Head-Gordon, C. Gonzales, and J. A. Pople, GAUSSIAN94, Gaussian, Inc, Pittsburgh, PA, 1995.

[57] Extensible Computational Chemistry Environmental Basis Set Data Base, Version 10 (1996).

[58] D. J. Millen, Can. J. Chem. **63**, 1477 (1985).

[59] G. E. Ewing, J. Phys. Chem. **91**, 4662 (1987).

[60] R. Schinke, *Photodissociation Dynamics* (Cambridge University Press, Cambridge, England, 1993).

[61] S. G. Lias, J. E. Barmess, J. F. Liebman, J. L. Holmes, R. D. Levin, and W. G. Mallard, J. Phys. Chem. Ref. Data Suppl. **17**, 1 (1988).

[62] D. K. Bohme, G. I. Mackay, and H. I. Schiff, J. Chem. Phys. **73**, 4976 (1980).